AIAA JOURNAL
Vol. 30, No. 3, March 1992

High Resolution Computation of Unsteady Flows in Pulsed Lasers

B. Srivastava,* F. Faria-e-Maia,† J. Her,‡ and J. Moran§
Avco Research Laboratory, Everett, Massachusetts 02149

A three-dimensional total variation diminishing (TVD) algorithm is developed for computing unsteady/steady flows in pulsed lasers. The general approach utilizes a three-dimensional thin-layer Navier-Stokes/Euler solver with source terms in the main channel, a one-dimensional Euler solver with source terms in the sidewall-muffler backing volume, and a quasisteady channel to backing volume flow-exchange model. Explicit time integration of these equations is accomplished via symmetric TVD formulations in an effort to enhance accuracy of the computed solution. Shock-tube experiments are performed to generate a data base for generic laser related problems and are shown to compare well with the computed solutions. Some aspects of laser flow/acoustic design are then discussed to demonstrate the capability of the code to supplement an overall flow system design effort.

Nomenclature

a = acoustic speed
C_d = discharge coefficient (muffler wall)
K_{ml} = normalized linear resistance in muffler backing volume, $K_m L/\rho_r u_r$
K_{mn} = normalized nonlinear resistance in muffler backing volume, $K_{mn} L$
K_r = normalized linear resistance of muffler wall, $K_r/\rho_r u_r$
L = reference length
p = dimensional pressure
t = dimensional time
u_r = reference velocity, a_0
α = open area ratio (muffler wall)
γ = ratio of specific heats
ρ_r = reference density, ρ_0

I. Introduction

FOR both excimer and IR pulsed lasers, improvements in the pulse-to-pulse beam quality lead to an increase in the effectiveness of the laser beam in achieving its specified objectives at the target. Pulsed excimer lasers are expected to yield higher average output power, whereas pulsed CO_2 lasers for radar application are expected to enhance their range and Doppler discrimination abilities if significant improvements in their pulse-to-pulse beam quality/frequency fidelity are realized. Significant improvements in the laser cavity medium homogeneity (that lead to improved beam quality/frequency fidelity) are possible through an understanding of critical issues that contribute to effective means of flow control and acoustic suppression on a pulse-to-pulse basis.

Recent advancement of computational techniques and computer speeds has provided an opportunity for rapid critical design evaluations that can supplement the overall laser flow system design. Several past technical efforts[1-7] in this area suggest the utility of such predictive approaches. A brief summary of these efforts is described in order to put the content of this paper in proper perspective.

Early computational methods in this area were restricted to quasi-one-dimensional approaches[1,2] based on either a characteristic scheme with discontinuity fitting[1] or a discontinuity capturing scheme using a convective algorithm like the sharp and smooth transport algorithm (SHASTA).[2] These computational methods employed spatially averaged time-dependent conservation equations in the sidewall-muffler backing volume. Backing volume losses were incorporated by developing approximate spatially averaged conservation equations assuming a certain velocity profile in the muffler baffles.[8] Several successful computations and their validations were reported in well-controlled validation experiments[8,9] for both approaches.

The need to develop two-dimensional computational approaches for such problems brought forth a series of studies[10] in an effort to identify a suitable two-dimensional algorithm and models. At the time, proven existing discontinuity capturing algorithms, such as those of MacCormack,[11] Beam and Warming,[12] and SHASTA,[13] were investigated for suitable laser-related model problems.[10] Because of coding complexity, two-dimensional characteristics schemes were not investigated further. These studies suggested that a convective algorithm like SHASTA is superior to the other schemes just noted.[10] Two-dimensional SHASTA codes were then evolved that were primarily inviscid in nature. Sidewall-muffler backing volume models were improved to include the full Euler equations with source terms.[10] This algorithm, however, suffered from several other deficiencies for laser applications. Computationally, this algorithm was found to be a factor of 2, or more expensive to run than the conventional explicit MacCormack's scheme. It was also found that this scheme typically required a very low Courant-Friedricks-Lewy (CFL) number for accurate solutions. Rapidly expanding grids to simulate large flow systems caused numerical difficulties. Inclusion of two-dimensional viscous effects would have made the computational procedure very expensive. A two-dimensional viscous computational procedure was then developed utilizing a more robust conventional MacCormack scheme.[11] In an effort to evolve a proper explicit damping procedure, a large number of code validation tests were performed.[7] These tests indicated excellent comparisons with velocity and pressure data. The predicted density field, however, was suspect due to numerical resolution of contact surfaces. It was, thus, recognized that further algorithm improvement is necessary to correct this deficiency. This, however, must be done by an appropriate tradeoff between computational cost and numerical accuracy.

Received June 11, 1990; presented as Paper 90-1508 at the AIAA 21st Fluid Dynamics, Plasma Dynamics, and Lasers Conference, Seattle, WA, June 18–20, 1990; revision received Jan. 3, 1991; accepted for publication Jan. 28, 1991.

*Principal Research Scientist, 2385 Revere Beach Parkway; currently, Deputy General Manager, HAL, Bangalore, India. Member AIAA.
†Scientist, 2385 Revere Beach Parkway.
‡Senior Scientist, 2385 Revere Beach Parkway.
§Principal Research Scientist, 2385 Revere Beach Parkway. Member AIAA.

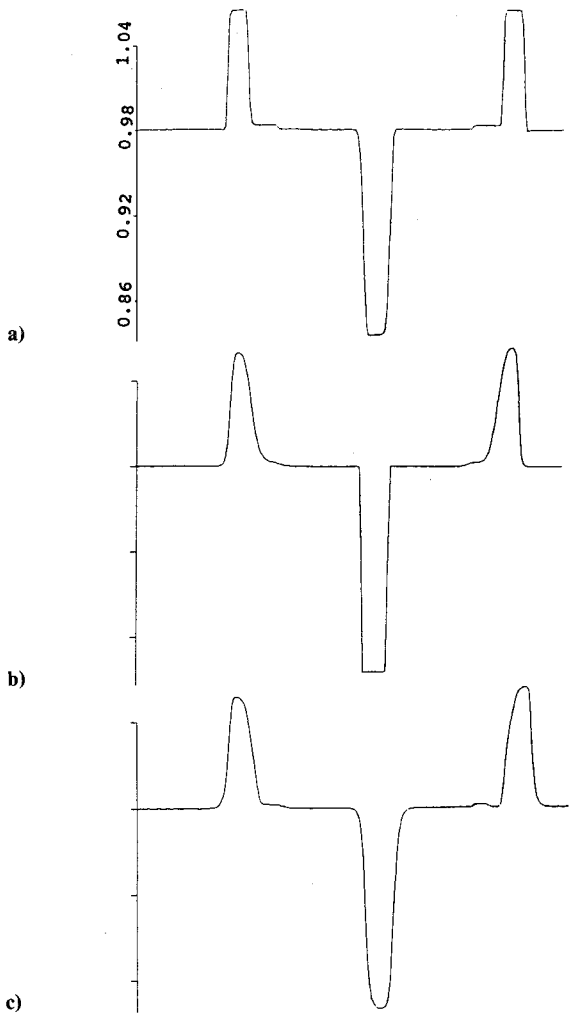

Fig. 1 Computed density pulse shape for three TVD schemes, Δx = 0.1, L = 6.4, CFL = variable: a) Chakravarty and Osher[14]; b) Harten[15]; c) Davis.[16]

Considerable progress has been made recently in the development of advanced high-resolution algorithms that are based on either total variation diminishing (TVD) or flux corrected transport (FCT) schemes. An objective of this paper is to evaluate currently available advanced high-resolution numerical schemes in both categories for laser-related problems with a purpose to identify a suitable scheme that optimizes computational cost and its attendant numerical accuracy. A similar detailed study of numerical issues related to algorithm, geometric, and boundary treatment errors was discussed in Ref. 10. Algorithm considerations, however, were restricted to early numerical methods.

The need for three-dimensional flow simulations for laser applications has recently been growing due to increased interest in large aperture discharge pumped pulsed CO_2 laser systems as well as Raman amplifiers in the excimer laser area. For the former, the axial waves generated in the optical direction due to the inactive volume (no pumping) between the discharge edge and the optical window may become an important consideration to ensure efficient multipulse discharge operation. In such cases, expansion in the flow direction, acoustic reverberation in the anode/cathode direction, and propagation in the optical direction lead to a truly three-dimensional wave phenomenon. This picture becomes even more complex in the presence of a cavity muffler, which is sometimes required to damp cavity transverse (anode-cathode) waves. This cavity muffler also acts on the waves moving in the optical direction. Thus, a cavity-muffler design based primarily on the transverse wave damping criterion may not be sufficient to ensure effective acoustic attenuation. A second objective of this paper is to study the time evolution and characteristics of the three-dimensional wave generated in the laser cavity in an effort to identify critical issues pertinent to the overall laser flow system design.

II. Algorithm Studies

Recent advances in high-resolution numerical techniques offer an alternative to enhance accuracy for the same grid sizes. Thus, an attempt was made to review and assess the available high-resolution numerical techniques for laser-related applications. During this effort, the primary objective was to enhance the accuracy of predicting density fields while minimizing the computational cost. A large number of numerical schemes and a variant thereof were tested on two one-dimensional laser related problems: one was the convection of a passive hot slug of gas and the other was a constant volume instantaneous heating process as encountered in a laser cavity and subsequent acoustic clearing process. A summary of the scheme studied, along with the relevant conclusions, is described next to highlight the final selection process. Two general basic categories of schemes were chosen. These two categories of schemes cover all advanced numerical schemes available to date.

A. Total Variation Diminishing Schemes

Rapid advances in high-resolution schemes have been possible through TVD concepts. The following schemes were evaluated in this category.

1. Total Variation Diminishing Scheme Based on Approximate Riemann Solver[14]

In our numerical studies on the model problems discussed earlier, we found this scheme to be the most accurate scheme for resolving pressure pulses. Figure 1a shows the density pulse shape computed by using this scheme for the constant volume instantaneous heating problem. Compare this computed pulse shape with other schemes shown later. This scheme, however, is computationally expensive and also works best at CFL = 0.4. Thus, computational cost is an issue.

2. Second-Order Upwind Total Variation Diminishing Scheme[15]

This scheme derives its origin from the theory of characteristics even though it is not based on an approximate Riemann solver. Figure 1b shows the computed pulse shape for the same problem at approximately the same time level as before. The pressure pulses are somewhat diffusive as compared to scheme 1. However, we found this scheme to be most accurate for the resolution of contact interfaces, as shown in Fig. 1b.

3. Lax-Wendroff Vector Total Variation Diminishing Scheme[16,17]

This scheme is based on characteristic directions and can allow a different limiter for the linearly degenerate case (i.e., contact surfaces). Figure 1c shows the computed pulse shape using this method for the same problem noted earlier. Our numerical experiments suggest that no additional advantage is observed if a highly compressed limiter is used for density fields.

4. Lax-Wendroff Scalar Total Variation Diminishing Scheme[16]

This and the previous TVD schemes are also called MacCormack TVD schemes. It is primarily intended to add a TVD-based damping term to the widely used two-step MacCormack scheme. The damping term in this scheme is scalar in character and does not preserve the characteristics nature. The results for this case were found to be the same as those shown in Fig. 1c.

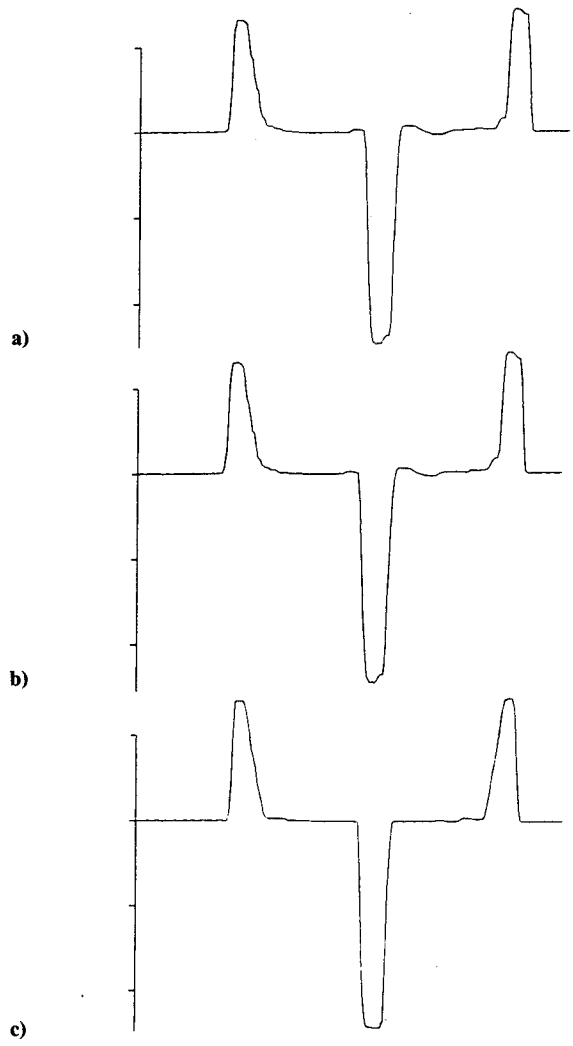

Fig. 2 Computed density pulse shape for three FCT schemes: a) SHASTA with Boris's limiter[18]; b) SHASTA with Zalesak's limiter[19]; c) SHASTA with Boris's limiter using entropy conservation.

B. Flux Corrected Transport Schemes

This scheme was originally proposed by Boris and Book[18] and later generalized by Zalesak.[19] The character of this general class of scheme is considerably different from the schemes described earlier. The following schemes were evaluated in this category.

1. Sharp and Smooth Transport Algorithm (SHASTA)

This is a convective algorithm and its major strength lies in the design of a specific limiter that operates as a diffusive and an antidiffusive step. Both Boris and Book's[18] and Zalesak's[19] limiters were evaluated. Figures 2a and 2b show the computed pulse for the two limiters. Notice from these figures that Zalesak's limiter is better than Boris and Book's limiter, but it is also associated with large unphysical perturbations behind the pulse. Both schemes display considerable overshoots near the contact interface. This overshoot can be eliminated by utilizing an entropy formulation for governing equations.[20] Figure 2c shows such a computational result. The result shown in Fig. 2c is remarkably superior to those shown in Figs. 2a and 2b for the same scheme. Notice also that Fig. 2c is quite close to Fig. 1a for the contact interfaces. However, expansions appear to be more spread out than the original formulation.

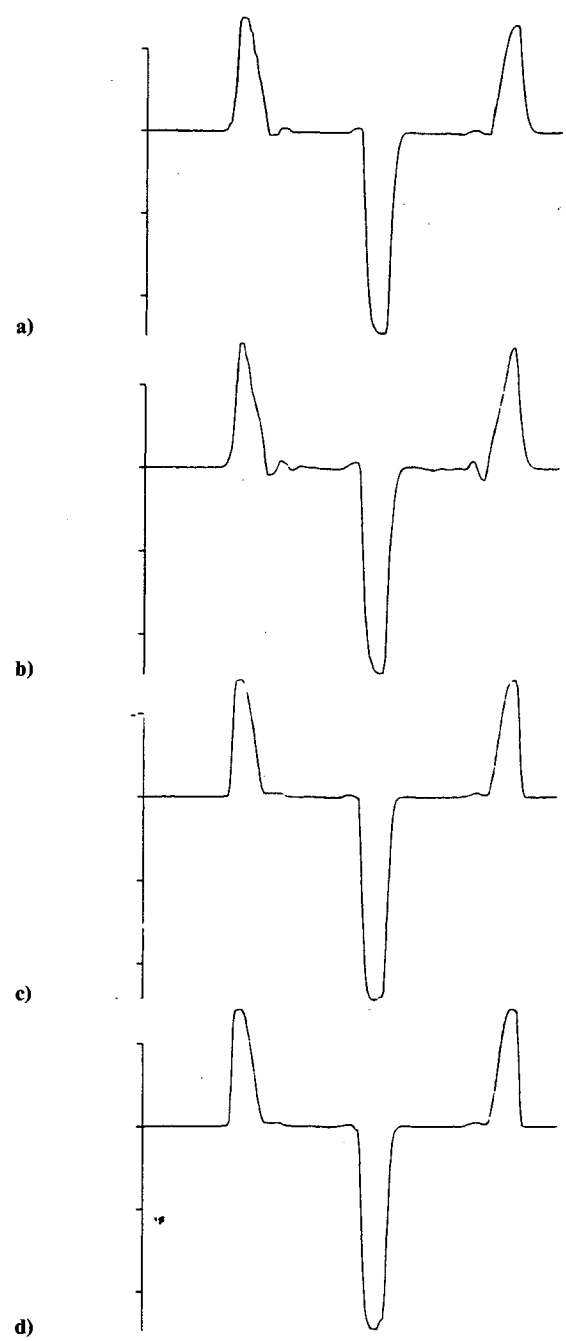

Fig. 3 Computed density pulse shape for Zalesak's schemes: a) second order with Boris's limiter; b) second order with Zalesak's limiter; c) fourth order with Zalesak's limiter; d) eighth order with Zalesak's limiter.

2. Zalesak's Flux Blending Scheme

Zalesak's generalizations[19] of the original Boris and Book's scheme[18] allow one to utilize a suitable combination of a lower- and higher-order scheme with either Boris and Book's limiter or Zalesak's limiter.[19] We have tested this scheme using Rusanov's first-order scheme[19] as the lower-order scheme and a second-order (Figs. 3a and 3b), a fourth-order[19] (Fig. 3c), and an eighth-order[19] (Fig. 3d) scheme as the higher-order scheme in the flux blending procedure. Higher spatial accuracy in Zalesak's scheme tends to reduce the overshoot associated with contact interface but only at the expense of considerably higher cost. These are evident in Figs. 3a–d.

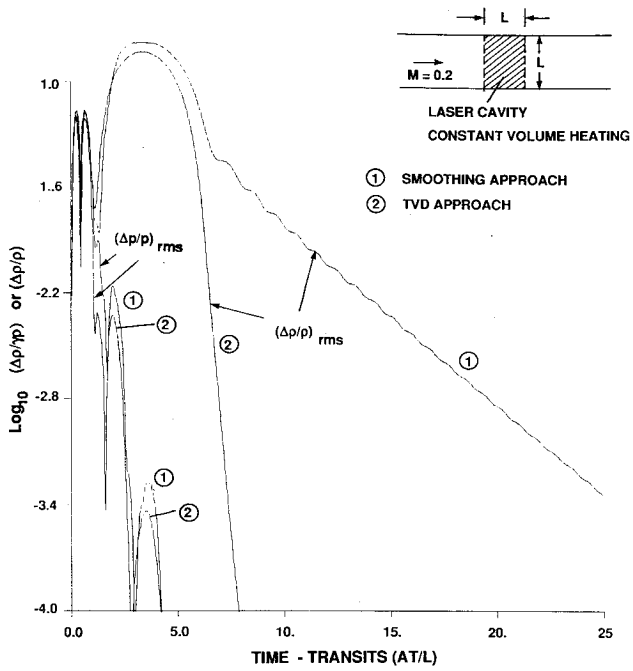

Fig. 4 Comparison of the two numerical schemes for a laser related idealized model problem.

Based on the studies just outlined, it is quite evident that the scheme presented in Fig. 1a is the best that can be obtained using the current state of the art. This scheme preserves the outgoing pulse shape accurately. However, the contact interfaces are slightly diffusive. The scheme shown in Fig. 1b is better for contact interfaces, but it seems too diffusive for outgoing pressure pulses. An entropy-based SHASTA algorithm appears to be also good for contact interfaces, but this scheme is also diffusive for expansions. All of these algorithms are considerably more expensive both from operation count standpoint and CFL limitations. On the other hand, TVD formulation based on Davis'[16] scalar approach (see Fig. 1c for computed pulse shape) appears to be a good compromise between accuracy and cost. This scheme is very easy to implement in the current code and appears to give a reasonable pulse shape.

Figure 4 shows a comparison of density predictions using the previous scheme and a new TVD scheme in terms of clearing of density homogeneity in a laser cavity after a pulse for a parallel hardwall case. Notice from this figure that almost 3 orders of magnitude improvement is achieved using the new scheme. It is also noteworthy from this figure that the new scheme does show some smearing of contact interfaces. Such smearing, however, can be controlled by grid refinement to yield the desired accuracy.

III. Governing Equations and Numerical Method

The three-dimensional conservation equations written in a transformed body-fitted coordinate system can be written in a generalized form as

$$\frac{\partial U}{\partial t} + \frac{\partial F}{\partial x} + \frac{\partial G}{\partial y} + \frac{\partial H}{\partial z} = S \tag{1}$$

where U is the state vector and S represents the source term related to channel loss terms. The transformed flux terms are given as F, G, H in the generalized coordinate directions x, y, and z.

The present approach utilizes the three-dimensional turbulent Navier-Stokes/Euler equations to describe the flow/acoustic motions in the main channel, whereas the backing depth of the sidewall muffler is described by the unsteady one-dimensional Euler equations with source terms. These source terms represent linear and nonlinear source terms typical of a porous material.[7] The muffler walls are treated by a quasisteady model for flow through orifices.[7] For further details of the governing equations, muffler model, and appropriate boundary conditions, the reader is referred to Refs. 1, 7, and 21.

It is convenient to describe the chosen numerical method for a one-dimensional system of hyperbolic conservation laws of the form

$$\frac{\partial U}{\partial t} + \frac{\partial F(U)}{\partial x} = 0 \tag{2}$$

The one-step explicit algorithm for this is given as

$$U_J^{n+1} = U_J^n - \lambda\,(H_{J+1}^n - H_{J-1}^n) \tag{3}$$

where

$$H_{J+1}^n = \tfrac{1}{2}\,(F_J^n + F_{J+1}^n - R_{J+1/2}\,\phi_{J+1/2}^l) \tag{4}$$

$$\phi_{J+1/2}^l = [\lambda(a_{J+1/2}^l)^2\,Q_{J+1/2}^l + \psi(a_{J+1/2}^l) \times (1 - Q_{J+1/2}^l)]\,\alpha_{J+1/2}^l \tag{5}$$

$$\alpha_{J+1/2}^l = R_{J+1/2}^{-1}\,\Delta_{J+1/2}\,U \tag{6}$$

$$\lambda = \Delta t/\Delta x$$

$$\Delta_{J+1/2}\,U = U_{J+1} - U_J$$

$$a^l = \text{eigenvalues of } A = \frac{\partial F}{\partial U}$$

In this definition, $R(R^{-1})$ is defined as the matrices whose columns are right (left) eigenvectors of $A(A^{-1})$, ψ is a function of a_{J+1}^l whose form will be defined later, and Q_{J+1}^l is the flux limiter. A few points of Eq. (5) are worth noting. When $Q_{J+1/2}^l = 1.0$, then Eq. (3) can be shown to be reduced to the classical one-step Lax-Wendroff scheme. Thus, for the one-step Lax-Wendroff scheme:

$$\phi_{J+1/2}^l = \lambda(a_{J+1/2}^l)^2\,\alpha_{J+1/2}^l \tag{7}$$

The second term of Eq. (5) is primarily the form that is utilized to obtain a TVD version of the Lax-Wendroff algorithm. The two-step method that we have utilized in this paper is derived from this one-step method.

The two-step method is given as

$$U_J^{(1)} = U_J^n - \lambda\,(F_{J+1}^n - F_J^n)$$

$$U_J^{(2)} = \tfrac{1}{2}\,[U_J^n + U_J^{(1)} - \lambda\,(F_J^{(1)} - F_{J-1}^{(2)})]$$

$$U_J^{n+1} = U_J^{(2)} + R_{J+1/2}^{(2)}\phi_{J+1/2}^{(2)} - R_{J-1/2}^{(2)}\phi_{J-1/2}^{(2)} \tag{8}$$

where the elements of vector $\phi_{J+1/2}^l$ are given as

$$\phi_{J+1/2}^l = \tfrac{1}{2}\,[\{\psi(a_{J+1/2}^l)\,\lambda - (\nu_{J+1/2}^l)^2\}\{1 - Q_{J+1/2}^l\}]\,\alpha_{J+1/2}^l$$

$$\nu_{J+1/2}^l = \lambda\,a_{J+1/2}^l$$

$$\psi\,(a_{J+1/2}^l) = |a_{J+1/2}^l| \tag{9}$$

The limiter function $\phi_{J+1/2}^l$ can take several forms, as evidenced in the literature.[15-17] The algorithm shown in Eq. (8) is based on characteristics requiring evaluation of the product $R\phi$ for every grid point. Note also that, since $Q_{J+1/2}^l$ is a user selected flux limiter, one has the freedom to choose different

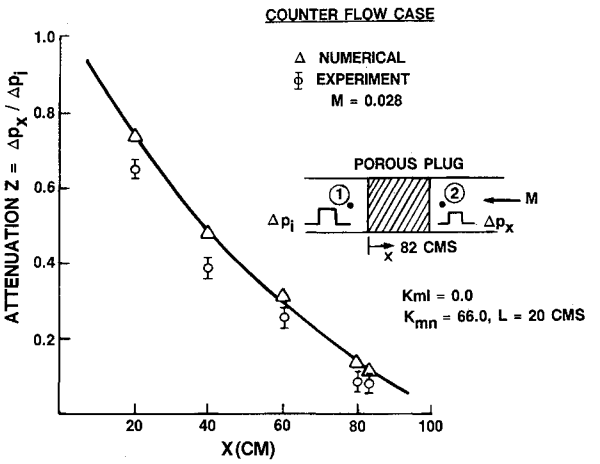

Fig. 5 Comparison of computations and experimental data for the attenuation of an input pulse through a porous plug for counterflow case; shows attenuation of the leading edge of input wave.

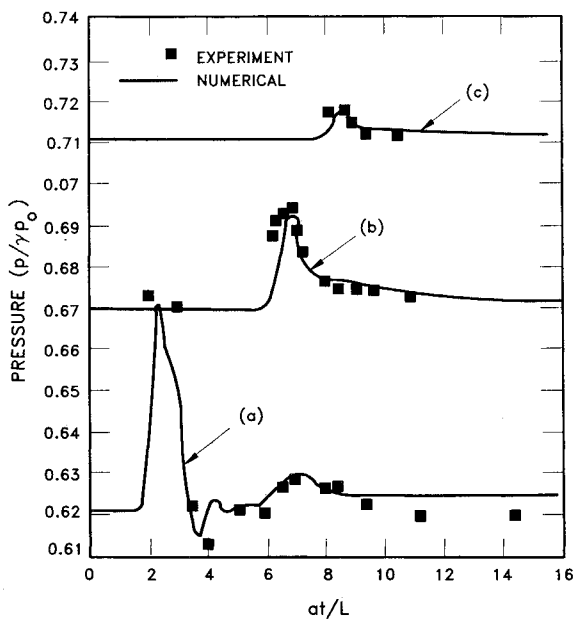

Fig. 6 Comparison of computations and experimental data showing response of the porous plug shown in Fig. 5 for counterflow case; exit pressures are shown for $M = 0.028$: a) inlet, at location 1, Fig. 5; b) midpoint of porous plug; c) exit, at location 2, Fig. 5.

limiters for different characteristics field. Requirements for shock resolution sometimes are different from those of contact interfaces. In such cases, this algorithm allows one to tailor the algorithm for a given problem. Computational cost of this algorithm, however, is high. It is sometimes more relevant to simplify this algorithm with a reasonably good numerical solution. This simplification is described next:

$$R_{J+1/2}\phi_{J+1/2} = \tfrac{1}{2}\{R_{J+1/2}\nu^l_{J+1/2}R^{-1}_{J+1/2} - R_{J+1/2}\,(\nu^l_{J+1/2})^2 \times (1 - Q^l_{J+1/2})\,R^{-1}_{J+1/2}\}\,\Delta_{J+1/2}\,U$$

Assuming a chosen scalar value for $\nu^l_{J+1/2}$ and $Q^l_{J+1/2}$:

$$R_{J+1/2}\phi_{J+1/2} = \frac{\nu}{2}(1 - \nu)(1 - Q_{J+1/2})\,\Delta_{J+1/2}\,U \qquad (10)$$

where the Courant number ν can be defined as

$$\nu = \max_J [\lambda_J]\,\frac{\Delta t}{\Delta x} \qquad (11)$$

The final forms of this scalar algorithm are given as[16]

$$R_{J+1/2}\phi_{J+1/2} = K\,(r^+_{J+1/2}, r^-_{J+1/2})\,\Delta_{J+1/2}\,U$$

$$R_{J-1/2}\phi_{J-1/2} = K\,(r^+_{J-1/2}, r^-_{J-1/2})\,\Delta_{J-1/2}\,U$$

with

$$K_{J+1/2}\,(r^+_{J+1/2}, r^-_{J+1/2}) = 0.5\,c(\nu)\,[1 - Q_{J+1/2}] \qquad (12)$$

$$Q_{J+1/2} = [\phi(r^+_{J+1/2}) + \phi(r^-_{J+1/2}) - 1]$$

$$c\,(\nu) = \nu\,(1 - \nu) \quad \text{if} \quad \nu \le 0.5$$

$$= 0.5 \quad \text{if} \quad \nu > 0.5$$

The definitions of $r^+_{J+1/2}$ and $r^-_{J+1/2}$ are somewhat arbitrary. Other forms have been proposed by several other authors. In our definitions, we utilize

$$r^+_{J+1/2} = \frac{(\Delta U_{J-1/2},\ \Delta U_{J+1/2})}{(\Delta U_{J+1/2},\ \Delta U_{J+1/2})}$$

$$r^-_{J+1/2} = \frac{(\Delta U_{J+1/2},\ \Delta U_{J+3/2})}{(\Delta U_{J+1/2},\ \Delta U_{J+1/2})} \qquad (13)$$

$$\Delta U_{J+1/2} = U_{J+1} - U_j \qquad \text{etc.}$$

$$\phi = \min\,(2\,r,\ 1) \quad \text{if} \quad r > 0$$

$$= 0 \quad \text{if} \quad r \le 0 \qquad (14)$$

where $(\Delta U_{J-1/2},\ \Delta U_{J+1/2})$ denotes the inner product of the components.

IV. Comparison with Experiments

An important and relevant code validation test relates to the response of a porous material for an input wave typically encountered in laser applications. We have conducted a code validation test using a square wave input on a porous material (characterized by linear and nonlinear losses). A similar test case was reported before[7] where we had studied the problem in a shock tube at flow Mach numbers of $M = 0$ and 0.026. For the latter case, the flow and the shock were moving in the same direction, i.e., a coflowing case. The case of counterflow, i.e., shock moving in a direction opposite to the flow, was studied recently. Typically, a flow-through absorber placed upstream of a laser cavity encounters a counterflow situation, whereas one placed downstream encounters a coflow situation. The response of the two absorbers is expected to be different due to varying internal resistive effects (resistive effects are directly related to the local velocity). Figures 5 and 6 show the comparison of the computed and shock-tube results. In Fig. 5, the results are presented in terms of attenuation of the square pulse ($\Delta p_x/\Delta p_i$) vs distance traveled through the porous material. Details of the porous material characteristics are also shown in Fig. 5. Although the overall decay rates appear to compare well, there were certain questions relating to accuracy of the data. This is reflected in the error bars in the data, as shown in Fig. 5. Figures 6a–c show a comparison of the computed inlet, midway, and exit pressure variation, respectively, with time for the same porous plug as compared to the experimental measurements. The magnitude of the reflected and transmitted pulses through the porous material as well as their temporal variations compare well with the measurements.

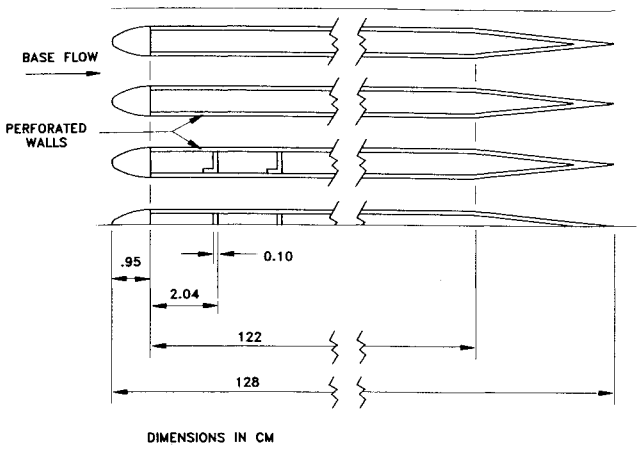

Fig. 7a Geometry for computational model derived from the shock-tube test sample.

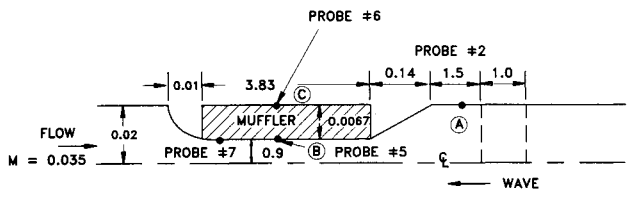

Fig. 7b Computational model utilizing symmetry conditions (dimensions are normalized).

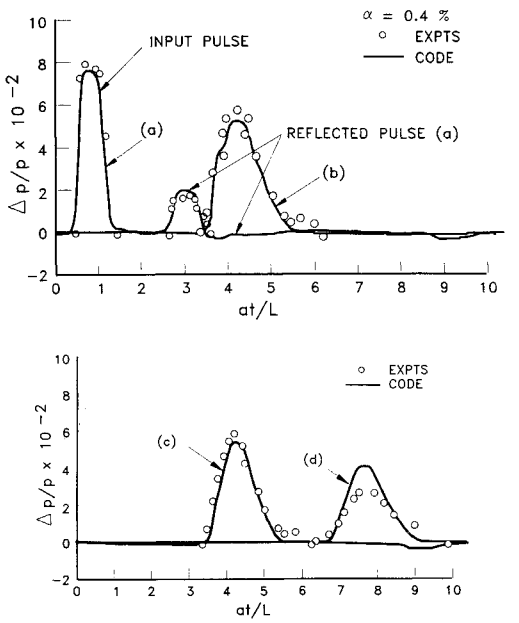

Fig. 8 Comparisons of the predicted pressure and experimental data for a) Probe #2 at location A as shown in Fig. 7b and b) Probe #5 at location B, Fig. 7b. Comparisons of the predicted pressure and measured data for c) Probe #6 at location C as shown in Fig. 7b and d) Probe #7, near muffler exit in Fig. 7b.

Figures 7 show the sketch of a segment of a flow-through muffler that has been tested in a shock tube. The relative dimensions of this muffler as well as its geometrical details are shown in Fig. 7a. The upstream end of this muffler provides a smooth entry to the incoming flow, whereas the exit is designed to minimize the wake arriving at the cavity. Figure

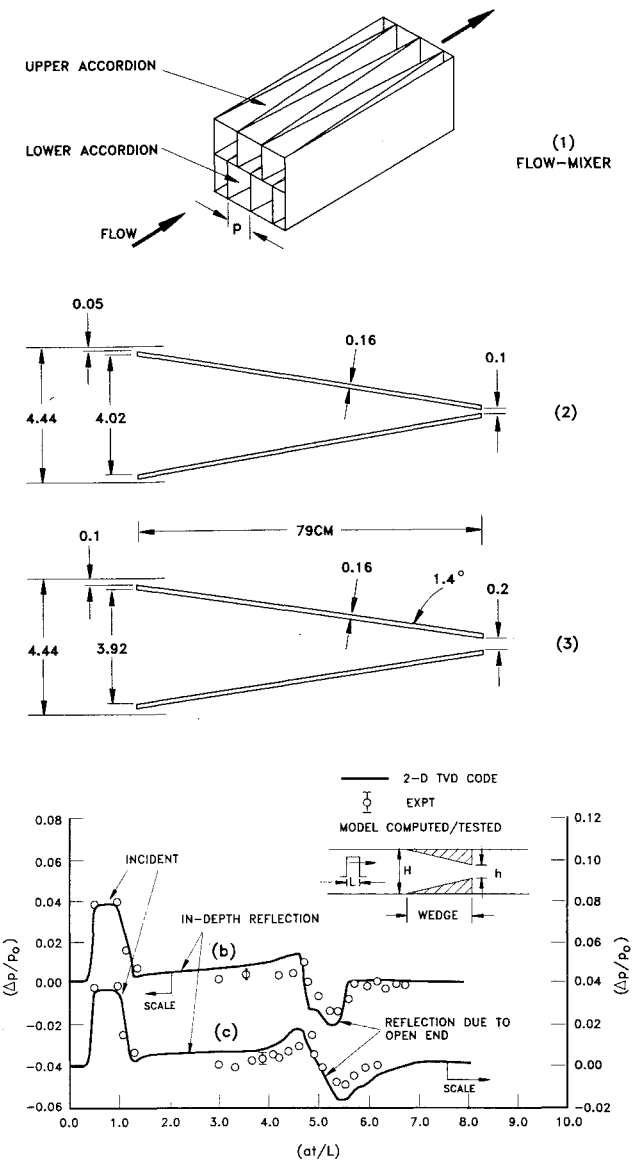

Fig. 9 a) Two shock-tube test models for acoustic evaluation of flow-mixer, 1) geometry of flow-mixer, 2) 40:1 area ratio wedge model, 3) 20:1 area ratio wedge model. Comparisons of incident and reflected waves for b) 20:1 wedge area ratio (H/h) at an incident wave overpressure ratio of 0.04 and c) 40:1 wedge area ratio at an incident wave overpressure ratio of 0.04.

7b shows a complete muffler configuration. Symmetric segments of this muffler system (as shown in Fig. 7a) were tested in the shock tube to assess its attenuation effectiveness. Computational calibration was also planned during this effort. Figure 7b also shows the location of the pressure probes (microphones) that were used to compare the computational and experimental results. Figures 8a–d show the results of the comparison. Figure 8a shows the comparison at the entrance of the muffler (i.e., probe 2). Notice that the input pulse into and the reflected pulse from the muffler compare well with experiments. Figures 8b and 8c show the same result for probe 5 and probe 6 (Fig. 7b). Good comparison with experimental data is obtained. Notice also from Figs. 8b and 8c that the response of the backing volume due to the channel pressure is almost instantaneous. Figure 8d shows a similar result at the exit of the muffler, i.e., probe 7. A significant discrepancy in the computed pressure is observed. The computed peak pressure appears to be higher even though its temporal duration is well predicted. The mechanism for this discrepancy

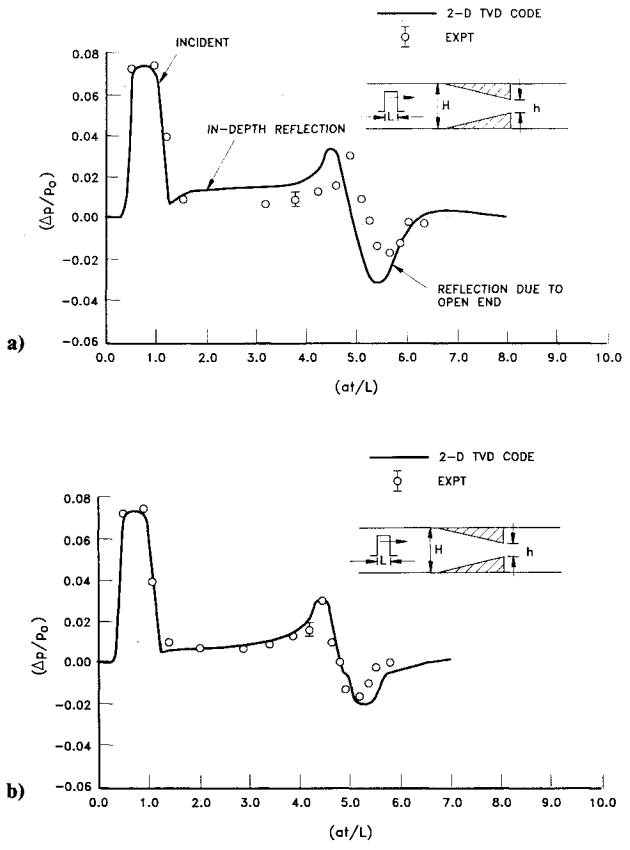

Fig. 10 Comparisons of incident and reflected waves for a) 40:1 wedge area ratio (*H/h*) at an incident wave overpressure ratio of 0.08; b) same as (a) but with laminar viscous effects included.

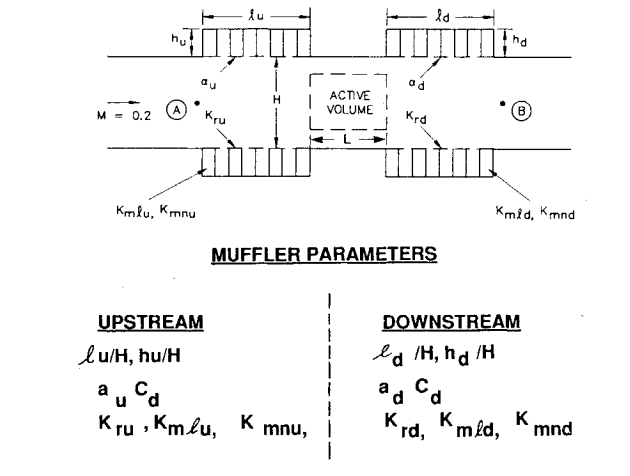

Fig. 11 Schematic of near cavity mufflers for damping longitudinal waves; all identified parameters are nondimensional.

appears to be due to viscous effects at downstream locations (when waves are weaker). This was not explored any further. On the whole, however, the predicted results are in good comparison with the shock-tube data.

Waves arriving at a flow mixer typically encounter a wedge in the direction of acoustic propagation (see Fig. 9a for sketch of the flow mixer). Area changes associated with such wedges are sources of wave redistribution and attenuation (caused by viscous effects in a narrow wedge) in a laser device. Sometimes with minor design modifications in a flow mixer one can accomplish acoustic redistribution of a desired nature. We will not elaborate here on various aspects of such a design but merely refer to it to point out our motivation to acoustically test two-dimensional wedges of very high area ratios (40:1 and 20:1). Figure 9b shows a comparison of the predicted and measured incident and reflected pressure profiles for a 20:1 open end wedge (see inset for details). For this case, the incident profile is a pressure pulse of overpressure ratio 0.04. Notice that this square pulse results in an in-depth compressive reflection (whose temporal duration is twice the acoustic transit time through the length of the wedge) and then a composite reflection due to an open end (sharp area change, i.e., 20:1). Figure 9c shows a similar result for a 40:1 area ratio with the same overpressure. In both cases, the computed results show a reasonable comparison with the data. Some of the differences in these two results can be attributed to viscous effects, as will be shown later. Figure 10a shows a comparison for an area ratio of 40:1 at an overpressure of ratio 0.08. For this higher overpressure, the computed expansion peak appears to be too large. There also appears to be a shift in the reflected wave arrival time. In an effort to address these issues, we computed the laminar viscous solution for the same problem. The intent was to assess the magnitude of the viscous dissipation on the predicted solution. Figure 10b shows a comparison of the computed viscous solution and the measured data. Notice that the viscous solution gives pressure distribution that compares very well with the experimental data. In retrospect, then, differences in computed and experimental data in Figs. 9b and 9c may also be attributed to viscous effects.

V. Two- and Three-Dimensional Applications Studies

In this section, we discuss the applications of the computational approach to demonstrate the extent such design tools can be utilized for optimizing laser system acoustic performance and also for identifying critical issues that relate to the overall flow system design.

Waves generated in the laser cavity are conveniently separated into longitudinal, transverse, and axial components. A detailed study of the transverse wave decay and its control/attenuation via a cavity muffler was presented in Ref. 7. Longitudinal waves have been studied in the past using either one-dimensional codes or linear analysis,[1,2] but a full discussion of the logic of a sidewall-muffler design using a two-dimensional validated code in relation to the acoustic requirements of a laser system has not been presented before. In this paper, we first illustrate this procedure to demonstrate a unique capability that can effectively assist in an overall design process. Later we assess the nature of three-dimensional axial waves in a laser cavity.

Figure 11 shows a schematic of a near cavity sidewall-muffler arrangement. A large number of parameters are seen to be involved whose selection must be based on a certain set of preassigned design requirements. Typically, such design requirements are 1) muffler volume compactness, 2) desired acoustic attenuation during an interpulse time, and 3) considerations of entropy generations at remote drag and heat transfer elements. This set of design requirements translates to constraints on the sidewall-muffler parameters. A typical design process optimizes such parameters to satisfy these three constraints. We will illustrate this procedure through parameter optimization studies for a given operating condition.

Figure 12 shows the results of an optimization study for arriving at the optimum value of open-area ratio. Values of other parameters were fixed at $K_r = 0.05$, $K_{ml} = 1.0$, $K_{mn} = 0.0$, $h/H = 0.5$, $C_d = 0.6$, and $l/H = 5.0$. Figure 12 shows the wall pressure at the upstream end of the upstream muffler (location A, Fig. 11) illustrating the nature of the transmitted wave through the upstream muffler. An optimum value of $\alpha_u/\alpha_d = 0.15/0.22$ is quite obvious from these results. This optimum follows directly from physical arguments that, at higher open-area ratios, the recompression wave caused

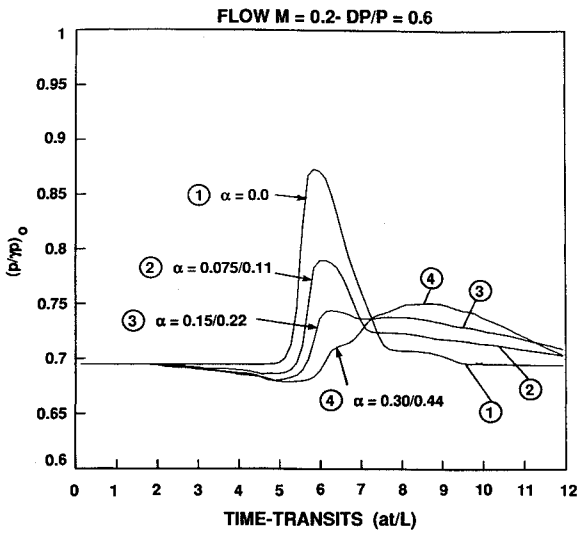

Fig. 12 Wall pressure variation with time at location A, Fig. 11, for various values of the upstream/downstream muffler open-area ratio showing pressure pulse transmitted through the upstream muffler.

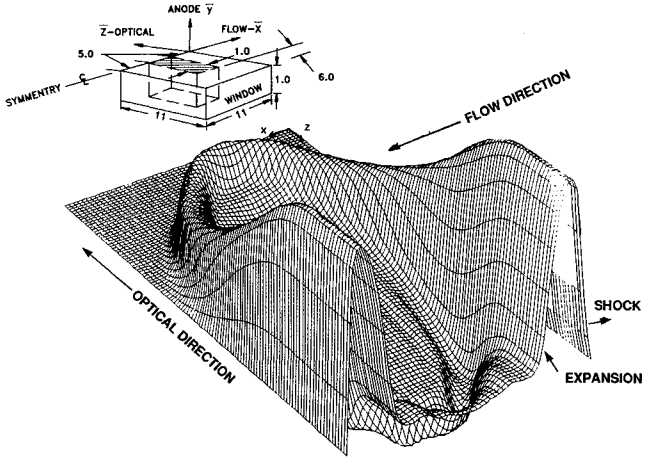

Fig. 13 Three-dimensional pressure plot for a hardwall laser cavity showing flow direction (longitudinal) and optical direction (axial) acoustic waves. Details were obtained at $t = 2.0$, $y = 0.5$.

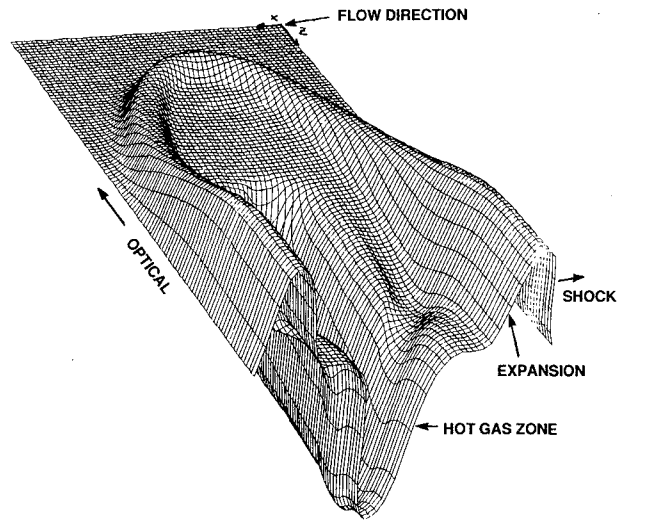

Fig. 14 Density plot corresponding to the case shown in Fig. 13. Thermal interface is seen as a sharp drop in density. Longitudinal waves are much weaker on the edges due to axial wave effects.

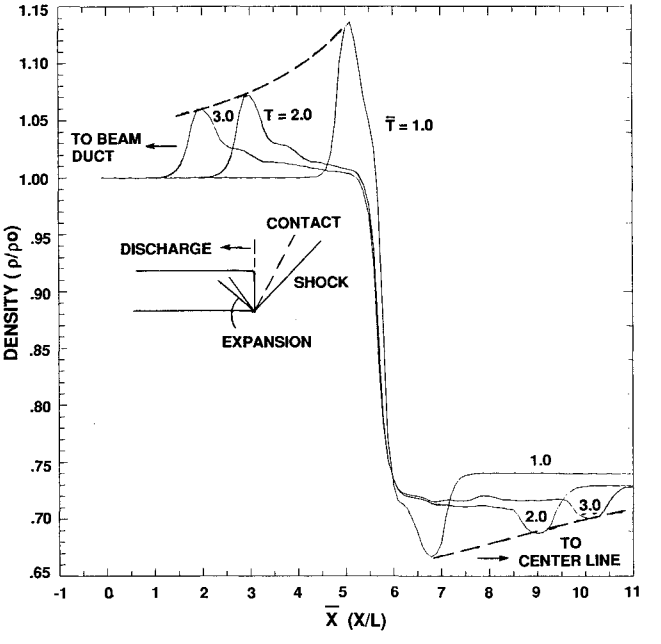

Fig. 15 Time evolution of the density profile showing decay rates of waves moving in the optical direction.

by the muffler is stronger. This is quite obvious from Fig. 12, which shows that while the lead shock strength decreases with increasing open area ratio the strength of the tail increases.

Similar optimization studies can be performed for all other parameters shown in Fig. 11. For lack of space, these results are not presented or discussed here. The results of Fig. 12, nonetheless, illustrate the utility of the code in assisting in a design process.

As pointed out before, waves generated in the optical direction may be of interest for many laser applications. Its primary impact is on discharge operation since they may cause preferential arcing paths through low-density regions of the laser cavity. This study was undertaken to accomplish the following objectives: 1) to determine interpulse laser cavity wave nature and its magnitude in the axial (i.e., optical) direction, and 2) to assess the extent of hot gas propagation in the optical direction toward the optical window/mirror/laser beam duct. Considerations of window/mirror damage and hot gas influx into the beam duct require such information.

It is relevant to point out here that this paper is not concerned with the management of such waves if its interpulse strength is unacceptably high. This subject matter will be discussed in a forthcoming paper. The primary objective of this study is to apply our three-dimensional code capability to assess the effects described earlier in a generic sense. Specific applications for a laser system design is beyond the scope of the present paper.

Figures 13–15 show an example of a three-dimensional inviscid unsteady computation for laser deposition problem where longitudinal (flow direction) and axial (optical direction) waves are present. Transverse waves were not included in this computation. The computations were performed on a $56 \times 6 \times 111$ ($n_x\ n_y\ n_z$) uniform grid where x is in the flow direction, y is in the anode to cathode direction, and z is in the optical direction. Because of symmetry, only half of the problem in the z direction was simulated. Thus, in this simulation, the left z-direction boundary is taken to be a symmetry boundary, whereas the right z-direction boundary is an optical window. Figures 13 and 14 show the computed results for pressure and density, respectively, on the x-z plane ($y = 0.5$) at a time $t = 2.0$. Many interesting features of the wave

pattern are visible at this time. Notice from Fig. 13 that the wave moving toward the optical window is a square pulse followed by a pressure ramp. There is also a left moving square pulse that tends to overexpand the cavity. The region between the two pulses is patched by a pressure ramp. This is a more complex wave pattern than previously realized. It appears that the cavity overexpansion occurs primarily due to the wave expansion process in the optical direction. The extent to which these waves influence the laser cavity performance depends on the details of the optical system design, length in the optical direction, and wave interaction with optical window/beam duct. For example, for short optical lengths, the tilted window walls would provide a mechanism for wave reflection effects during an interpulse time. Such advantages would not be possible for long optical lengths where waves travel only a fraction of the total optical lengths. In the latter case, management of these waves needs to be addressed via either controlling the amplitude of the initial wave strength or by utilizing a well-designed cavity muffler. Figure 14 shows a density plot in the x-z plane for the same case showing the effects of gas heating and the associated thermal interfaces. The density field in this figure shows the thermal interface and also the relevant forward moving waves. Figure 15 shows the time evolution of the density, indicating clearly that the hot gas interface does not propagate significantly in the optical direction. The fractional length (relative to cavity flow direction length) is expected to be nearly ~ 0.1 at this overpressure (i.e., $\Delta p/p \sim 0.6$). For most typical applications, therefore, the hot gas expansion in the optical direction is not expected to be an issue.

VI. Conclusions

This paper deals with the development of a high-resolution three-dimensional code for the computation of flowfield in a laser environment. In an effort to select an optimum algorithm relative to its cost and accuracy, a series of laser related model problems are first studied using various TVD and FCT algorithms. Based on these studies, an existing two-dimensional code is extended to three-dimensional flows with TVD formulation. The TVD formulation yields higher computational accuracy for the same grid sizes. A series of computational comparisons with in-house shock-tube experiments are then made to show good overall flow predictive capability of the code.

Computational studies have been performed to illustrate the utility of the code in supplementing a laser flow system design process for optimum parameter selection. Specific examples include the studies for the optimum design of near-cavity sidewall mufflers for attenuating longitudinal waves in the context of an overall laser flow system design. A three-dimensional wave evolution process in the laser cavity has also been studied for the first time in an effort to understand the overall picture of the pressure distribution in the laser cavity. These results and similar studies provide useful design information that is being utilized for overall flow system compactness and improved cavity performance.

Acknowledgments

The experimental tests and code validation tests of Sec. V were conducted at Avco Research Laboratory (ARL) under Contract F29601-84-C-0091 sponsored by the Air Force Weapons Laboratory. The remainder of the work reported in this paper was sponsored by the Independent Research and Development funds of Ground Based Laser program office at ARL. The authors are indebted for financial support in this area from both.

References

[1]Srivastava, B. N., Knight, C. J., and Zappa, O. L., "Acoustic Suppression in a Pulsed Laser System," *AIAA Journal*, Vol. 18, No. 5, 1980, pp. 555–562.

[2]Ausherman, D. R., Alber, I. E., and Baum, E., "Acoustic Suppression in a Pulsed Chemical Laser," *AIAA Journal*, Vol. 17, No. 5, 1979, pp. 490–497.

[3]Srivastava, B. N., "Pressure Wave Attenuation due to Anode Mufflers in Pulsed Lasers," *AIAA Journal*, Vol. 21, No. 3, 1983, pp. 381–389.

[4]Thayer, W. J., III, Buonadonna, V. R., and Sherman, W. D., "Pressure Wave Suppression for a Pulsed Chemical Laser," AIAA Paper 78-1216, July 1978.

[5]Kulkarny, V. A., et al., "Modeling Acoustic Suppression in Pulsed Gas Laser Systems," AIAA Paper 82-0891, June 1982.

[6]Srivastava, B. N., and Vu, B. T., "Pulsed CO_2 Acoustic Modelling," Presented at 1987 IRIS Active Systems Specialty Group Conference, Orlando, FL, Oct. 1987.

[7]Srivastava, B. N., et al., "Computation of Inviscid/Viscous Flowfield in Pulsed Lasers," *AIAA Journal*, Vol. 26, No. 10, 1988, pp. 1254–1262.

[8]Morris, J., et al., "Further Investigations of Flow and Acoustics in Pulsed Excimer Laser," Poseidon Research Rept. No. 32, Santa Monica, CA, Aug. 1980.

[9]Tong, K. O., Knight, C. J., and Srivastava, B. N., "Interaction of Weak Shock-Waves with Screens and Honeycombs," *AIAA Journal*, Vol. 18, No. 11, 1980, p. 1298.

[10]Srivastava, B. N., Cruickshank, J., and Moran, J., "Numerical Schemes for the Computation of Unsteady Flow in Pulsed Lasers," *AIAA Journal*, Vol. 25, No. 6, 1987, pp. 845–854.

[11]MacCormack, R. W., "The Effect of Viscosity in Hypervelocity Impact Cratering," AIAA Paper 69-354, 1969.

[12]Beam, R. M., and Warming, R. F., "An Implicit Factored Scheme for the Compressible Navier-Stokes Equations," *AIAA Journal*, Vol. 16, No. 4, 1978, pp. 393–402.

[13]Boris, J. P., and Book, D. L., "Flux-Corrected Transport I, SHASTA—A Fluid Transport Algorithm that Works," *Journal of Computational Physics*, Vol. 11, 1973, p. 38.

[14]Chakravarty, S. R., and Osher, S., "A New Class of High Accuracy TVD Schemes for Hyperbolic Conservation Laws," AIAA Paper 85-0363, Jan. 1985.

[15]Harten, A., "High Resolution Schemes for Hyperbolic Conservation Laws," *Journal of Computational Physics*, Vol. 49, 1983, pp. 357–393.

[16]Davis, S. F., "TVD Finite Difference Schemes and Artificial Viscosity," ICASE Rept. No. 84-20, June 1984.

[17]Yee, H. C., "Construction of Explicit and Implicit Symmetric TVD Schemes and their Applications," *Journal of Computational Physics*, Vol. 68, 1987, pp. 151–179.

[18]Boris, J. P., and Book, D. L., "Flux Corrected Transport III, Minimum Error FCT Algorithms," *Journal of Computational Physics*, Vol. 20, 1976, pp. 379–431.

[19]Zalesak, S. T., "Fully Multidimensional Flux-Corrected Transport Algorithms for Fluids," *Journal of Computational Physics*, Vol. 31, 1979, pp. 335–362.

[20]Lewis, J. E., "Modeling Basis of the Poseidon One-Dimensional Laser Gas Dynamics Code," Poseidon Research Rept. No. 90, June 1987.

[21]Srivastava, B. N., Faria-e-Maia, F., Her, J., and Moran, J., "High Resolution Computation of 2-D/3-D Unsteady Flowfield in Pulsed Lasers," AIAA Paper 90-1508, June 1990.